Fault structure and seismogenic dynamics of the Feidong earthquake sequence, Anhui

xiang Su Zhang[1], wen Shi Xie[2], yao Guang Yin[3], and lei Jin Li[4]

[1]Shanghai Earthquake Agency
[2]Anhui Earthquake Agency
[3]University of Chinese Academy of Sciences
[4]China University of Geosciences Beijing

January 24, 2025

Abstract

This study investigates the seismogenic fault and dynamic origin of the Feidong earthquake sequence in Anhui. We used the improved DBSCAN algorithm to identify the fault geometry and structural characteristics, then integrated fault location, velocity structure, and focal mechanism data to invert the local stress state and fluid pressure distribution. The main findings are: (1) The earthquake sequence was triggered by a single seismogenic fault with a strike of 224.92° and dip angle of 82.41°, likely a right-lateral strike-slip segment of the Chihe-Taihu Fault. (2) The local stress field in the seismogenic region is dominated by a predominantly compressive strike-slip regime, with a significant clockwise rotation compared to the background stress field. This change may relate to seismic stress release, fault interactions, and high-pressure fluids. (3) Earthquakes mainly occurred at the boundary of high- and low-velocity regions, suggesting a stress accumulation zone, likely influenced by fluid dynamics. (4) The M[?] 4.7 earthquake generated 20 MPa of excess fluid pressure, with 80% of events experiencing pressures over 10 MPa. High-pressure fluids, particularly along the Chihe-Taihu Fault, played a significant role in triggering the sequence. (5) The seismogenic fault's instability coefficient of 0.73 indicates low stability. While the short-term risk of another earthquake is low, long-term stress accumulation and specific triggering environments pose a future seismic risk. This study offers valuable insights for seismic hazard assessments and the Tan-Lu Fault Zone's activity.

Hosted file

`manuscript.docx` available at https://authorea.com/users/883947/articles/1262412-fault-structure-and-seismogenic-dynamics-of-the-feidong-earthquake-sequence-anhui

Fault structure and seismogenic dynamics of the Feidong earthquake sequence, Anhui

Suxiang Zhang [1,2] , Shiwen Xie [3,4*], Guangyao Yin [5], Jinlei Li [6]

1 Shanghai Earthquake Agency，Shanghai 200062，China

2 Shanghai Sheshan Geophysics National Field Observation and Research Station，Shanghai 200062，China

3 Anhui Earthquake Agency，Hefei 230031，China

4 Mengcheng National Geophysical Observation, Earthquake Agency of Anhui, Mengcheng Anhui, 233500, China

5 School of Earth and Planetary Sciences, University of Chinese Academy of Sciences, Beijing, 100049, China

6 School of Geophysics and Information Technology, China University of Geosciences, Beijing 100083, China

Abstract This study aims to reveal the geometric parameters of the seismogenic fault and its dynamic origin for the Feidong earthquake sequence in Anhui. By precisely locating the catalog and applying the improved DBSCAN algorithm to automatically identify the fault geometry, we determine its structural characteristics. Subsequently, by integrating fault location, velocity structure, and focal mechanism data, we invert the local stress state and excess fluid pressure distribution in the seismogenic region. The results indicate the following: (1) The Feidong earthquake sequence was triggered by a single seismogenic fault, with a strike of 224.92° and a dip angle of 82.41°. It is inferred that this fault is a right-lateral strike-slip segment of the Chihe-Taihu Fault. (2) The local stress field in the seismogenic region is characterized by a σ_1 axis oriented approximately east-west (EW), and a σ_3 axis oriented approximately north-south (NS), with the maximum horizontal principal stress also oriented east-west. This suggests a predominantly compressive strike-slip stress regime, with a significant clockwise rotation compared to the background stress field. The change in the stress field may be related to seismic stress release, interactions between branch blind faults and the main fault, as well as high-pressure fluids. (3) The Feidong earthquake sequence primarily occurred at the boundary between high- and low-velocity regions, close to the low-Vs side, indicating that the earthquakes are located in a stress accumulation zone and possibly influenced by fluid dynamics. (4) The M_S4.7 Feidong earthquake generated excess fluid pressure of 20 MPa, with about 80% of the seismic events experiencing excess fluid pressures greater than 10 MPa. Combined with the low-Vs and high-Vp/Vs velocity structure in the seismogenic area, it is suggested that high-pressure fluids played a significant role in triggering the Feidong earthquake sequence. Fluids may have infiltrated the seismogenic area from the southwest along the Chihe-Taihu Fault and accumulated at depths of 0–15 km, causing localized overpressures. (5) The seismogenic fault in the regional stress field is prone to strike-slip failure, with its fault instability coefficient being 0.73, indicating a relatively low level of stability. Although the likelihood of a subsequent earthquake in the short term is small, the long-term accumulation of stress and specific seismic triggering environments suggest that there remains a risk of future felt earthquakes. This study provides important insights into the seismogenic structure and dynamic mechanism of the Feidong earthquake sequence and offers a reference for subsequent seismic

First author. Suxiang Zhang, master, assistant engineer, majors in seismogenic structure, focal mechanism and tectonic stress field, E-mail: zhangsuxiang@ecut.edu.cn
Corresponding author. Shiwen Xie, engineer, majors in seismic monitoring, E-mail: ECITxshw@163.com

hazard assessments in the seismogenic area and for studies on the activity characteristics of the southern segment of the Tan-Lu Fault Zone.

Keywords Feidong earthquake; Stress field characteristics; Focal mechanism solutions; Seismogenic structure; Dynamic origin

1 Introduction

According to the China Earthquake Networks Center, on September 18, 2024, at 20:08, an M_S 4.7 earthquake occurred in Feidong County, Hefei City, Anhui Province (31.98°N, 117.60°E), at a depth of approximately 10 km. The epicenter was located about 37 km from the center of Hefei. This earthquake was the largest recorded in modern history for Hefei, causing noticeable tremors in the city and nearby areas, such as Nanjing, Yangzhou, and Hangzhou (Ni et al., 2025). Prior to the mainshock, the region had already experienced three earthquakes with magnitudes greater than M_S 3.0: a M_S 3.5 earthquake on February 24, a M_S 3.1 earthquake on May 12, and a M_S 3.9 earthquake on September 14. Following the mainshock, aftershocks were relatively active, particularly the M_S 3.8 earthquake on September 25 and the M_S 3.3 earthquake on October 1. The earthquake sequence had a wide-reaching impact in the Yangtze River Delta region, attracting significant attention from various sectors of society. However, to date, systematic studies on the fault structure (e.g., fault geometry), seismogenic mechanism, and dynamic origin of the Feidong earthquake sequence remain insufficient and require further in-depth exploration.

The seismic activity in the Feidong region is likely closely related to its complex regional tectonic setting. As a major active tectonic unit in the region, the Tan-Lu Fault Zone has historically been associated with several moderate to strong earthquakes and exhibits continuous tectonic stress accumulation (Figure1 (a); Chen, 2023). Previous studies have shown that the Anhui segment of the Tan-Lu Fault Zone lies within an active tectonic stress field, influenced by interactions between multiple fault types. This interaction may lead to a complex seismic activity mechanism (Li et al., 2010; Zhang et al., 2010). Fault structure, as a key controlling factor for earthquake occurrence, significantly impacts the mechanical behavior of fault slip (Wan, 2020; Zhang et al., 2022; Liu et al., 2025). The Tan-Lu Fault Zone is characterized by a complex system of sub-faults, with a fault network that intersects and provides dynamic conditions for triggering or inducing large-scale earthquakes in the region (Hu et al., 2013; Shao et al., 2019; Ozawa et al., 2021). Therefore, an in-depth study of the detailed fault structure and seismogenic mechanism in the Feidong region is critical for understanding the dynamic processes underlying seismic activity in this area.

Although the M_S 4.7 Feidong earthquake has a relatively small magnitude, it is the largest earthquake ever recorded in the southern segment of the Tan-Lu Fault Zone. Such episodic earthquakes are typically characterized by strong unpredictability and uncertainty, and their seismogenic mechanisms often differ from those of typical tectonic earthquakes. Previous studies have shown that episodic earthquakes generally occur in regions with concentrated tectonic stress accumulation; however, their seismogenic mechanisms are not solely dependent on a single tectonic background or fault geometry. Instead, they are influenced by a combination of local geological conditions and fault mechanical characteristics. These factors include local stress accumulation, fault friction properties, fluid infiltration, and external disturbances (Barbot, 2019; Philibosian and Meltzner, 2020).

Currently, there have been some preliminary findings regarding the fault structure and

seismogenic mechanism of the Feidong earthquake sequence. For instance, Ni et al. (2025) based on the spatial distribution characteristics of the seismic sequence after precise location determination, tentatively inferred that the seismogenic structure is a fault with a NE strike and NW dip. Liu et al. (2015) using deep reflection profiles, revealed that the main fault (seismogenic area) of the Tan-Lu Fault Zone in the Anhui segment is vertically inserted into the surface, with a strike approximately NNE and a dip to the east, covered by thick sedimentary layers. However, neither study provided precise fault geometry parameters nor explored the seismogenic mechanism in detail.

This study first applies an improved DBSCAN algorithm proposed by Zhang et al. (2022) to automatically identify the seismogenic fault and its geometric parameters. The CAP method is then used to invert the focal mechanisms of earthquakes with magnitudes greater than or equal to M_L 4.0 (Yang et al., 2022), while the HASH method is employed to invert the focal mechanisms of earthquakes with magnitudes between M_L 2.5 and 3.9 (Hardebeck, 2002; 2003). Based on these results, the seismogenic fault plane is selected according to the geometric characteristics of the fault, and a spatial grid for stress field inversion is defined based on the fault location and velocity structure. The local stress state in the seismogenic area is then inverted using the linearization method proposed by Michael (1984) (Zhang et al., 2024). Additionally, this study utilizes the Focal Mechanism Tomography (FMT) method proposed by Terakawa et al. (2010) to assess the excess fluid pressure state on the seismogenic structure. Finally, by integrating velocity structure, local stress state, and excess fluid pressure analysis, this study aims to investigate the seismogenic mechanism of the Feidong earthquake sequence and its underlying dynamic origin. The systematic analysis of fault structure and dynamic causation in this study not only helps reveal the seismogenic mechanism in this region but also provides valuable scientific insight into the triggering mechanisms of similar earthquakes in the Yangtze River Delta and their potential seismic risk assessment.

2 Data and Method

2.1 Seismic catalog and velocity structure data

The study area is located between 31.5°N–32.5°N and 117°E–119°E. The Anhui Earthquake Agency has deployed 88 fixed stations (with epicentral distances ranging from 0 to 300 km) and 3 mobile stations (with epicentral distances ranging from 0 to 50 km). The seismic catalog data used in this study is sourced from the research by Ni et al. (2021), which includes 329 seismic events recorded between February 24, 2024, and November 6, 2024. These events were precisely located using the double-difference location method (HypoDD) based on waveform cross-correlation (Waldhauser and Ellsworth, 2000). The velocity structure data is derived from Zhang et al. (2023), who obtained a 3D velocity model for the southern segment of the Tan-Lu Fault Zone through joint inversion of surface wave and body wave arrival times. The horizontal grid spacing of the velocity structure is 0.5°, and the depth interval is 5 km.

2.2 Automatic fault identification

This study employs an improved DBSCAN algorithm for automatic fault identification (Zhang et al., 2022) to provide the spatial distribution and geometric parameters of the seismogenic fault of the Feidong earthquake sequence. The method performs multi-level

clustering from high-density to low-density layers, avoiding interference from manually selected parameters. The main steps of the algorithm are as follows: (1) Determine the threshold for the number of valid events based on the seismic catalog data. (2) Compute the distance matrix $D_{\mathrm{n\times n}}$ for the seismic catalog. (3) Sort each row of the distance matrix $D_{\mathrm{n\times n}}$ in ascending order and compute the average value of each column D_{K}, yielding D_{eps}. (4) Based on the mathematical expectation, calculate D_{minPts} corresponding to each D_{eps}. (5) Identify the optimal D_{eps} and D_{minPts}, then perform fault segment identification and fault parameter calculation. (6) For the remaining seismic data, repeat steps 2–5 until the number of seismic events identified in the cluster is below the threshold for valid events, at which point fault identification terminates. (7) Merge adjacent fault segments with similar parameters.

The improved DBSCAN automatic fault identification method proposed by Zhang et al. (2022) does not take depth into account when calculating distances, which may introduce some errors into the research results. To address this issue, this study adopts equation (1) to replace the original distance formula used in the method:

$$d = 2R \times arcsin\left(\sqrt{\sin\left(\frac{\varphi_2-\varphi_1}{2}\right)^2 + \cos(\varphi_1) \times \cos(\varphi_2) \times \sin\left(\frac{\lambda_2-\lambda_1}{2}^2\right) + ((z_2 - z_1)^2)}\right) \quad (1)$$

Where R is the Earth's radius; φ_1 and φ_2 represent the longitudes of two seismic events; λ_1 and λ_2 represent the latitudes of the two seismic events; z_1 and z_2 represent the depths of the two seismic events; and d is the distance to be calculated.

Based on the distance formula described above, this study performed multi-level clustering on the Feidong earthquake sequence in Anhui. Following the method's steps, only a single clustering iteration was conducted. The threshold for the number of valid events was set at 30, with the optimal K-value determined to be 13. The corresponding eps and minPts values were 0.084 and 19.90, respectively. Using these parameters, one valid fault was identified, with a total of 246 seismic events within the cluster.

2.3 Focal mechanism and stress field inversion

Based on the clustering results described above and the regional velocity structure provided by the USTClitho2.0 continental lithosphere model (Han et al., 2022), this study used the CAP method to invert the focal mechanisms of five earthquakes with magnitudes of M_{L}≥4.0. Additionally, the HASH method was employed to invert the focal mechanisms of 17 earthquakes with magnitudes between M_{L} 2.5 and 3.9 (Appendix table 1). During the selection process, focal mechanism solutions with uncertainties greater than 40° were excluded, resulting in 20 high-quality focal mechanism solutions. To evaluate whether the diversity condition of focal mechanism solutions is satisfied, this study adopted the approach proposed by Hardebeck and Hauksson (2001), which measures the root mean square (RMS) rotation angle between individual focal mechanism solutions and the average focal mechanism solution. The average error level of the focal mechanism solutions in this study is approximately 20°, with an RMS value of 48.4°, indicating that the dataset satisfies the diversity assumption.

The stress characteristics obtained from the inversion of focal mechanisms at different depth ranges vary (Luo et al., 2015; Zhang et al., 2024). However, because the seismic events in this sequence occurred within similar depth ranges and in the same velocity structure region, we infer that seismic activity in this area exhibits relatively uniform physical properties, thereby satisfying

the homogeneity assumption for stress field inversion. Consequently, this study did not subdivide depth ranges for spatial grid inversion of the stress field, but instead performed a unified inversion of the stress field (Custódio et al., 2016).

The double-couple focal mechanism model can provide two possible fault planes, which has led to the development of two commonly used methods for selecting the seismogenic fault plane: (1) selecting the fault plane whose slip direction is more consistent with the shear stress direction (Wan et al., 2016). (2) selecting the fault plane with a higher fault instability coefficient as the seismogenic fault plane (Vavryčuk et al., 2014). However, previous studies have shown that neither of these methods can accurately identify the seismogenic fault plane from the focal mechanism, which can consequently affect the results of stress field inversion (Li et al., 2024). Therefore, to select a fault plane that is closer to the true seismogenic fault plane, this study uses the normal angle between the two possible fault planes from the focal mechanism and the automatically identified seismogenic fault plane as the metric. The fault plane with the smaller normal angle is chosen as the true seismogenic fault plane. Based on this criterion, 20 seismogenic fault planes were selected, and the local stress tensor in the seismogenic area was inverted using the linearization method proposed by Michael (1984). The maximum horizontal principal stress direction corresponding to this stress field was calculated using the method proposed by Lund et al. (2007). Additionally, the uncertainty in the stress field parameters was assessed using the Monte Carlo algorithm. Through statistical analysis of multiple sampling and inversion results of the focal mechanism solutions, the following uncertainty estimates were obtained: the uncertainty of the three principal stress axes was 15°, and the uncertainty of the shape ratio (R-value) was 0.23.

2.4 Excess fluid pressure calculation

To evaluate excess fluid pressure near the seismogenic area, this study employs the Focal Mechanism Tomography (FMT) method proposed by Terakawa et al. (2010) and Terakawa et al. (2012). The basic assumptions of the FMT method include: (1) the fault strength $\boldsymbol{\tau}$ is controlled by the Coulomb failure criterion, $\boldsymbol{\tau = \mu(\sigma_n - \rho)}$, where $\boldsymbol{\sigma_n}$ is the normal stress, $\boldsymbol{\rho}$ is the excess fluid pressure, and $\boldsymbol{\mu}$ is the friction coefficient; (2) the fault slip direction is aligned with the shear stress direction; (3) the vertical principal stress is due to the overlying rock's gravitational force; and (4) the fault, in the current stress field, is at critical state under hydrostatic pressure, oriented along the optimal rupture direction.

3 Results and Discussion

3.1 Seismogenic mechanism and fluid control

The results of the focal mechanism inversion indicate that the earthquake sequence includes 7 strike-slip earthquakes, 2 normal strike-slip earthquakes, 2 reverse strike-slip earthquakes, 3 normal earthquakes, and 5 reverse earthquakes. Notably, all earthquakes with magnitudes $M_L \geq 4.0$ are strike-slip events, suggesting that the sequence is predominantly characterized by strike-slip ruptures (Figure 1(b)).

Based on the spatial grid division of the stress field inversion, the selection of the seismogenic fault plane, and the stress field inversion method outlined above, the local stress field

in the seismogenic area is inverted as follows: the azimuth and plunge of $\boldsymbol{\sigma_1}$ are 83° and 15°, respectively; the azimuth and plunge of $\boldsymbol{\sigma_2}$ are 328° and 58°, respectively; the azimuth and plunge of $\boldsymbol{\sigma_3}$ are 182° and 27°, respectively; the shape ratio *R* is 0.55, and the direction of the maximum horizontal principal stress is 86.2° (Table 1). These results suggest that the stress field is characterized by: a $\boldsymbol{\sigma_1}$ axis oriented approximately east-west (EW), a $\boldsymbol{\sigma_3}$ axis oriented approximately north-south (NS), indicating a predominantly compressive strike-slip stress regime (Figure 2(a-b); Guiraud et al., 1989). The direction of the maximum horizontal principal stress ($\boldsymbol{\sigma_{H_{max}}}$) is nearly horizontal and consistent with the right-lateral strike-slip activity observed in the seismogenic region (Figure 1(b)).

Xu (2022) used a combined focal mechanism approach to invert the stress field for a 1°×1° grid in Anhui Province, yielding a principal compressive stress direction of NE, which represents the average stress field in the study area. To quantitatively assess the differences between the local stress field in the seismogenic region and the background stress field, the Snoke method (Snoke et al., 1984; Snoke et al., 2003) was further applied to invert the focal mechanisms of 16 historical earthquakes in the region. Additionally, a joint iterative inversion method for tectonic stress field and fault identification (Vavryčuk et al., 2014) was used to invert the background stress field parameters (Table 1). The background stress field is characterized by: a $\boldsymbol{\sigma_1}$ axis oriented approximately NEE, a $\boldsymbol{\sigma_3}$ axis oriented approximately NNW, and a nearly horizontal plunge for the principal stress axis, consistent with a strike-slip stress regime (Figure 2(c-d)). Compared to the background stress field, the local stress field in the seismogenic area exhibits a notable clockwise rotation.

The results of crustal anisotropy inversion in the seismogenic area, based on near-field waveform data by Shi et al. (2022), show that the fast wave polarization direction at the station on the western side of the earthquake sequence (LAN) is oriented SEE, while the station to the east is oriented NE (Figure 1(a)). This also indicates that within a unified background stress field, there is a noticeable variation in the local stress field, exhibiting significant spatial heterogeneity in the stress distribution.

Martínez-Díaz (2002) suggested that the rotation of the local stress field may be related to the accumulation and release of regional tectonic stress. Chang et al. (2010) found that uneven sliding and shear forces at fault intersections can lead to changes in the local stress field. Rybicki et al. (1985) in their study of stress field variations caused by fault interactions, discovered that such interactions could distort the local stress field, creating rotational effects that significantly differ from the regional background stress field. The Feidong region exhibits a complex fault network system and seismic stress release. Therefore, this study hypothesizes that the heterogeneity of the local stress field may result from a combination of seismic stress release and the interaction between branch faults and the main fault. Additionally, the involvement of "high excess pressure fluids" may also play an important role in the changes to the stress field (Terakawa et al., 2010).

Previous studies have suggested that the interaction between fluid diffusion and fault geometry may control seismic activity (Yin et al., 2024; Liu et al., 2025). To further analyze the excess fluid pressure state in the seismogenic area, this study uses the Focal Mechanism Tomography (FMT) method to invert the excess fluid pressure of the seismogenic structure, based

on the local stress field parameters described above (Terakawa et al., 2010; 2012). The results show that the excess fluid pressure for the M_S 3.5 earthquake on February 24 and the M_S 3.8 earthquake on September 25 was approximately 37 MPa; for the M_S 3.9 earthquake on September 14 and the M_S 4.7 earthquake on September 18, it was around 20 MPa; and for the M_S 3.3 earthquake on October 1, the excess fluid pressure was nearly 0 MPa (Figure 3). Statistical analysis reveals that about 80% of the seismic events in the Feidong earthquake sequence had excess fluid pressures greater than 10 MPa. This result is highly consistent with the velocity structure characteristics of the seismogenic area: the low Vs and high Vp/Vs in the seismogenic region suggest the presence of widespread fluid-saturated fractures or pores near the fault plane (Figure 3). This high pressure fluid significantly weakened the frictional strength of the fault by reducing the effective normal stress on the fault plane, thereby triggering fault slip.

However, it is noteworthy that the entire earthquake sequence occurred on the side with relatively low Vs, and a significant low Vs and high Vp/Vs anomaly is observed along the AB survey line. This suggests the presence of fluid infiltration in the seismogenic area, with this phenomenon extending to a depth range of 0-15 km along the seismogenic fault. Combining the excess fluid pressure calculation results with the seismic environment at the boundary between high- and low-velocity regions, particularly the low Vs and high Vp/Vs characteristics, this study hypothesizes that the rupture in the seismogenic area was not only influenced by stress accumulation at the boundary between high- and low-velocity regions but may also have been triggered by the significant facilitation of fault slip due to high-pressure fluids.

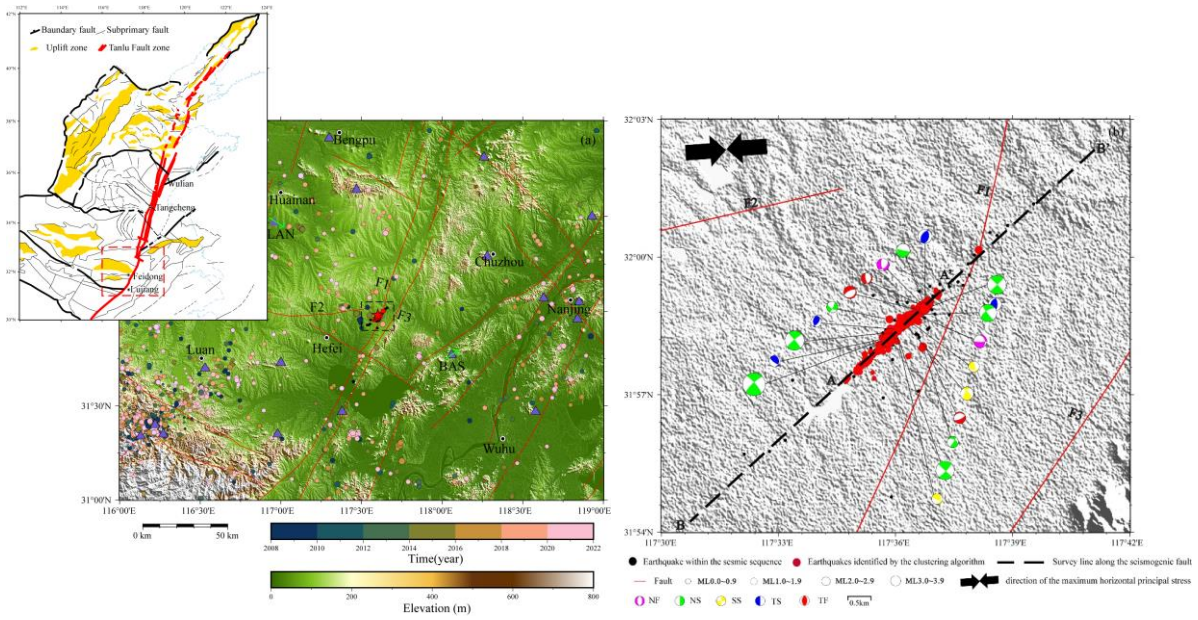

Figure 1. Tectonics of the Feidong area (a), spatial distribution of the earthquake sequence and fitted fault (b) (a) Blue triangles represent seismic stations, black circles represent city locations, and green arrows indicate the fast shear wave polarization direction at the stations. (b) F1: Chihe-Taihu Fault. F2: Gushi-Feizhong Fault. F3: Jiashan-Lujiang Fault.

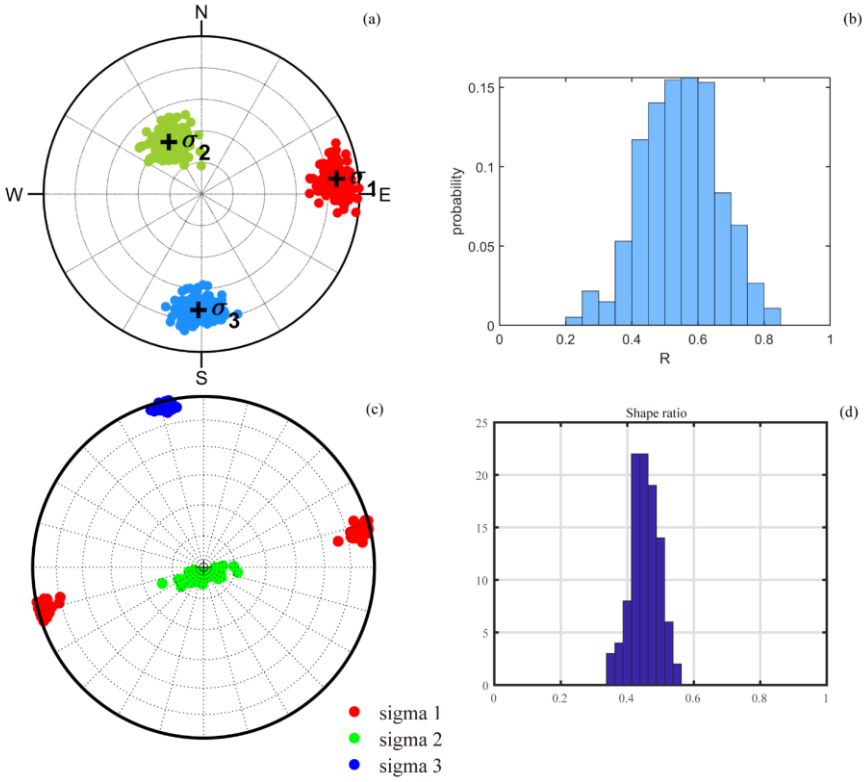

Figure 2. Inversion results of the local stress field in the seismogenic area (a-b) and the background stress field (c-d).

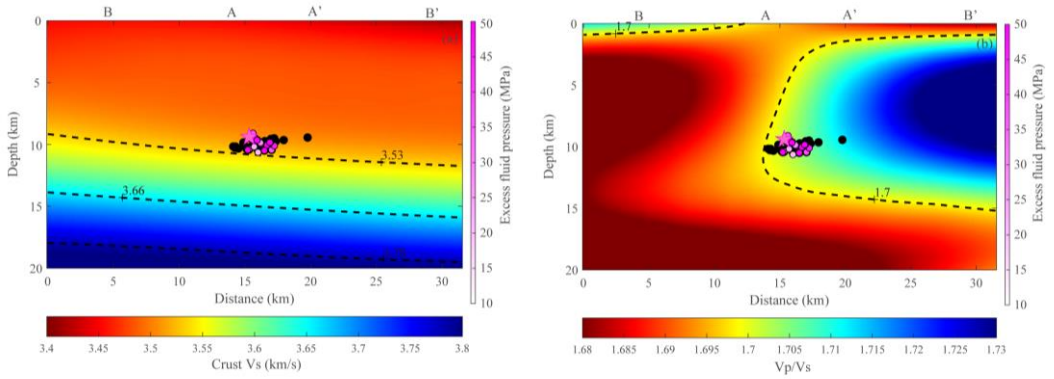

Figure 3. Vs (a) and Vp/Vs (b) velocity structure profiles along the survey line in Figure 1(b).
The pink pentagram represents the M_S 4.7 earthquake, and the black solid circles represent earthquakes with magnitudes $M_L \geq 2.0$ identified in the clustered seismic sequence.

Table 1 Stress field inversion results

Study Area	σ_1		σ_2		σ_3		shape ratio R	$\sigma_{H_{max}}$/(°)	Stress state
	azimuth /(°)	plunge /(°)	azimuth /(°)	plunge /(°)	azimuth/(°)	plunge/(°)			
local stress field	83	15	328	58	182	27	0.55	86.2	Stress-slip
background	76	5.4	222	84	345.7	3.6	0.48	75.9	Stress-slip

stress field

3.2 Seismogenic fault structure of the Feidong earthquake sequence, Anhui

The geometric parameters of the seismogenic fault obtained in this study are a strike of 224.92° and a dip angle of 82.41°, with standard deviations of 0.01 and 0.04, respectively (Table 2). The fault exhibits a NE strike and NW dip, with a high-dip three-dimensional structural characteristic (Figure 4). This result is largely consistent with the seismogenic structure identified by Ni et al. (2025) and the geometric characteristics of the main fault in the Anhui segment of the Tan-Lu Fault Zone (Liu et al., 2015).

The epicentral region is located between the western edge of the Hefei Basin and the southern segment of the Zhangbaling Uplift, controlled by the Tan-Lu Fault Zone. The main tectonic units include the NE-striking Chihe-Taihu Fault (F1), the nearly EW-striking Gushi-Feizhong Fault (F2), and the NE-striking Jiashan-Lujiang Fault (F3). Among these, the Chihe-Taihu Fault and the Jiashan-Lujiang Fault are the main faults in the Anhui segment of the Tan-Lu Fault Zone (Figure 1). Deep reflection profiles show that these faults are vertically inserted into the surface, displaying a flower-like structure with a tectonic distribution characterized by alternating uplift and depression (Li et al., 2020).

The results of this study indicate that the seismogenic fault of the Feidong earthquake sequence is highly consistent with the geometric characteristics of the main fault in the Anhui segment of the Tan-Lu Fault Zone. It exhibits a NE strike, NW dip, and a high-dip right-lateral strike-slip fault. Considering the regional geological context and the parameters of the seismogenic fault, it is hypothesized that the seismogenic fault is likely an active segment of the Chihe-Taihu Fault. Its fault properties, geometric characteristics, and mode of activity align with the actual observed results.

The direction of the maximum horizontal principal stress is nearly orthogonal to the strike of the seismogenic fault, suggesting that the fault may be in a state of dominant control within the local stress field (Figure 1(b)). This is consistent with the direction of the principal compressive stress (NNE) in the regional background stress field and the overall strike-slip seismic activity in the area, reflecting the typical interaction between the regional stress field and fault geometry. However, the fitted strike of the seismogenic fault (224.92°) deviates significantly by approximately 25° from the known surface trace of the Chihe-Taihu Fault (Figure 1(b)). This study hypothesizes that the main reasons for this discrepancy are: (1) Rotation of the local stress field: The local stress field in the seismogenic area exhibits a clear clockwise rotation compared to the background stress field, which may cause the activity direction of the local fault to differ slightly from the trace direction of the regional main fault (Faulkner et al., 2006). (2) Inconsistencies in fault geometry at different depths: The geometry of the deeper segments of the fault may deviate from the trace direction of the shallow segments due to tectonic evolution or shear effects (Zion and Sammis, 2003). Such discrepancies between deep and shallow fault geometries are common in complex fault networks (Morley and Nixon, 2016).

The significant discrepancy (25°) between the fitted strike of the fault and the surface trace of the main fault suggests that the seismogenic fault is more likely to be a blind branch fault rather than a synthetic fault of the main fault. Blind faults are typically located around the periphery of the main fault system, with their activity influenced by local stress concentration and elevated fluid pressure. This study found excess fluid pressures as high as 50 MPa in the seismogenic area, with fluids potentially infiltrating deep blind faults along the Chihe-Taihu Fault. These fluids preferentially act on the weak planes of the blind faults, significantly reducing the effective normal stress and ultimately triggering fault slip (Terakawa et al., 2010; Ellsworth, 2013). The high permeability and low friction strength of the blind fault further enhance the fluid-triggered mechanism. In contrast, if the seismogenic fault were a synthetic fault of the main fault, its activity would more likely be controlled by background tectonic stress rather than such a significant fluid influence. However, the comprehensive results of this study indicate that the dominant role of high-pressure fluids in fault slip further supports the hypothesis that the seismogenic fault is a blind branch fault.

In summary, this study proposes the following possible dynamic causes for the Feidong earthquake sequence: (1) The boundary between high- and low-velocity regions provides the medium conditions for accumulating significant strain energy in the seismogenic area, facilitating energy release and forming the foundational environment for the seismic activity; 2) Regional tectonics (such as the Chihe-Taihu Fault) provide the primary pathway for the migration of deep fluids toward shallower regions. Fluids migrate upward along the fault, where they are trapped and accumulated at the boundary between high- and low-velocity regions. This accumulation significantly promotes slip along the blind branch faults by reducing the effective normal stress on the fault; 3) The elevated stress level in the seismogenic area leads to further accumulation or dynamic migration of fluids along the fault. This excess fluid pressure weakens the frictional strength of the fault, increasing the likelihood of seismic triggering and slip instability. Therefore, the dynamic cause of the Feidong earthquake sequence is likely to be largely controlled by the synergistic interaction between excess fluid pressure and the local stress field. Additionally, this study hypothesizes that the deep fluids may originate from mantle degassing or magmatic hydrothermal activity (Fu, 2021), dehydration release from hydrous minerals in the lithosphere (e.g., chlorite, serpentine), or the deep accumulation of shallow pore fluids within the fault system (Kim et al., 2023).

This study employs the fault instability coefficient I proposed by Vavryčuk et al. (2014) to assess the stability of the seismogenic fault in the Feidong earthquake sequence (Wang et al., 2019), and projects the local stress field in the seismogenic area onto the fault to determine its primary rupture mode (Figure 5; Wan, 2020). The calculation results show that the seismogenic fault is prone to strike-slip ruptures, with an instability coefficient (fault slip tendency) of 0.73, indicating a relatively low fault stability (Appendix figure 1). The influence of high-pressure fluids not only triggered the earthquake sequence but may also exacerbate the fault's instability and the complexity of rupture. Although the mainshock released some stress, the likelihood of subsequent earthquakes in the short term is small. However, the long-term accumulation of stress and the specific seismic triggering environment may still lead to felt earthquakes.

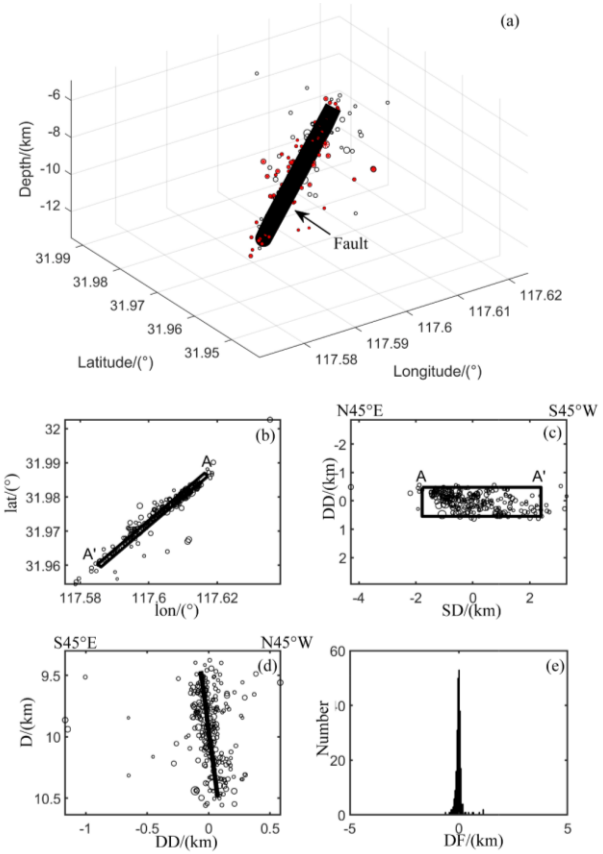

Figure 4. Clustering and Fault Plane Determination of the Feidong Earthquake Sequence.

a) Earthquakes identified within the seismogenic fault plane by the clustering algorithm, marked in red; b) Projection of the earthquakes onto the horizontal plane; c) Projection of the earthquakes onto the fault plane; d) Projection of the earthquakes onto the cross-sectional plane perpendicular to the fault plane; e) Distribution of small earthquakes' distances to the fitted fault plane.

Here, SD represents strike, DD represents dip, and DF represents the distance from small earthquakes to the fault plane.

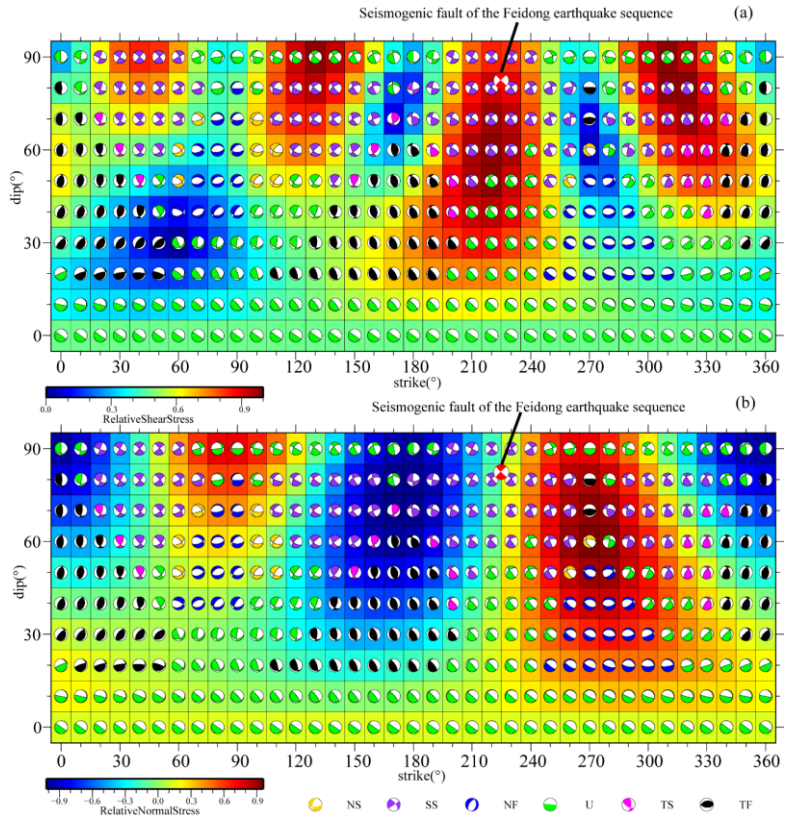

Figure 5. Relative shear stress, normal stress, and rupture mode of the seismogenic fault under the local stress field in the seismogenic area

Table 2 Fault parameters of Feidong earthquake sequences determined in this study

Number of Earthquakes within the Cluster	Fault Strike /(°)	Fault Dip/(°)	Coordinates of the four vertices of the fault plane (Longitude/°E, Latitude/°N, Depth/km)	Relative Shear Stress	Relative Normal Stress
246	224.92	82.41	117.6174, 31.9861, 9.4645 117.6164, 31.9870, 10.4794 117.5851, 31.9604, 10.4794 117.5861, 31.9595, 9.4645	0.884	-0.559

4 Conclusion

This study utilizes the precisely located catalog of the Feidong earthquake sequence and combines the improved DBSCAN algorithm to automatically identify the seismogenic structure and its fault parameters (Figure 4; Table 2). The focal mechanisms were inverted using the CAP and HASH methods, based on waveform data provided by the Anhui Seismic Network (Appendix table 1). The seismogenic fault plane was further selected based on fault parameters, and reliable stress field parameters were inverted. Finally, the local stress field in the seismogenic area was projected onto the seismogenic fault, and the relative shear and normal stress magnitudes were calculated (Figure 5; Table 2). By integrating the velocity structure and fluid overpressure (Figure 3), the dynamic origin and subsequent seismic hazard of the Feidong earthquake sequence were analyzed in detail. The main conclusions of the study are as follows:

(1) Seismogenic Fault Characteristics: The seismogenic structure of the Feidong earthquake sequence is a single fault, with a strike of 224.92° and a dip angle of 82.41°. Considering the regional geological context, it is inferred that this fault is a right-lateral strike-slip segment of the Chihe-Taihu Fault.

(2) Stress Field Characteristics of the Seismogenic Area: The local stress field in the seismogenic area is characterized by a σ_1 axis oriented approximately east-west (EW), a σ_3 axis oriented approximately north-south (NS), and the maximum horizontal principal stress also oriented east-west. This stress field exhibits a predominantly compressive strike-slip stress regime. Compared to the background stress field (with σ_1 oriented NEE and σ_3 oriented NNW), the stress field in the seismogenic area shows a clear clockwise rotation. The variation in the stress field may be related to seismic stress release, the interaction between branch faults and the main fault, and the influence of high-pressure fluids.

(3) Seismic Environment and Rupture Mechanism: The Feidong earthquake sequence is primarily concentrated in the boundary between high- and low-velocity regions, with a focus on the low-Vs side. This suggests that the area provides favorable conditions for the accumulation of significant strain energy, making it prone to rupture and stress release, with potential fluid influence.

(4) Excess Fluid Pressure Analysis: The excess fluid pressure associated with the M_S 4.7 Feidong earthquake is approximately 20 MPa, and about 80% of the seismic events in the Feidong earthquake sequence experienced fluid pressures greater than 10 MPa. Based on the low-Vs and high-Vp/Vs velocity structure characteristics in the seismogenic area, it is inferred that high-pressure fluids played a significant role in triggering the Feidong earthquake sequence.

Fluids likely infiltrated the seismogenic area from the southwest along the Chihe-Taihu Fault, accumulating within the 0–15 km depth range, creating localized fluid overpressures. This accumulation reduced the effective normal stress on the fault, thereby facilitating fault slip.

(5) Fault Stability and Long-Term Seismic Hazard: The seismogenic fault plane is prone to strike-slip rupture events within the local stress field, and its instability coefficient is 0.73, indicating a relatively low level of fault stability. Although the likelihood of a subsequent earthquake occurring on this fault in the short term is small, the long-term accumulation of regional stress, along with the influence of specific seismic triggering conditions (such as fluid overpressure and tectonic stress concentration), suggests that the Chihe-Taihu Fault still poses a high seismic risk in the medium to long term.

This study provides the first comprehensive analysis of the dynamic origin of the Feidong earthquake sequence, revealing the crucial role of high-pressure fluids in earthquake occurrence. The dynamic origin of the Feidong earthquake sequence is largely controlled by the synergistic interaction between high-pressure fluids and the local stress field. The boundary between high- and low-velocity regions provides an ideal environment for fluid accumulation and stress buildup, while the Chihe-Taihu Fault acts as a key fluid migration pathway, facilitating the upward movement and concentration of fluids. The study indicates that the triggering mechanism of the Feidong earthquake sequence is primarily governed by fluid overpressure and the heterogeneity of the regional stress field. These results provide important insights into the seismic activity of the southern segment of the Tan-Lu Fault Zone and offer a basis for assessing regional seismic hazard.

Although this study presents a dynamic origin analysis for fluid-triggered earthquakes, the specific source of the fluids still requires further investigation. Future work, utilizing advanced techniques such as background noise tomography (Fang et al., 2015) and double-difference tomography constrained by velocity ratio consistency (Guo et al., 2018), can provide higher-resolution 3D velocity models. These will offer more precise data support for understanding the impact of fluids on fault stability, the interaction between fluids and the regional stress field, and fluid migration pathways in the study area.

Declarations

Declaration of Conflict of Interest: All authors acknowledged that there is no conflict of interest on record.

Author Contributions: Conceptualization: Suxiang Zhang. Data curation: Shiwen Xie. Formal analysis: Suxiang Zhang, Guangyao Yin. Funding acquisition: Suxiang Zhang. Investigation: Suxiang Zhang, Shiwen Xie. Methodology: Guangyao Yin. Project administration: Suxiang Zhang. Resources: Shiwen Xie. Software: Suxiang Zhang, Guangyao Yin. Supervision: Guangyao Yin. Writing-original draft: Suxiang Zhang. Writing-review & editing: Guangyao Yin, Jinlei Li.

Funding

Shanghai Municipal Social Development Science and Technology Support Project (23DZ1203900); Shanghai Municipal Science and Technology Commission Research Program (23DZ1200200).

Acknowledgments

Some of the figures in this paper were created using GMT software (Wessel and Smith, 1991). We would like to thank Dr. Zhenyue Li from the Institute of Geology, China Earthquake Administration, and Researcher Yongge Wan from the Institute of Disaster Prevention Science and Technology for providing the programs used in this study. Additionally, we appreciate Researcher Ailan Zhu from the Shanghai Earthquake Bureau for providing fault data. We express our gratitude to all of them.

Data Availability Statement

The earthquake catalog data for the Feidong earthquake sequence used in this study can be accessed via DOI: https://doi.org/10.1016/j.eqs.2024.11.001. The 3D velocity structure data for the southern segment of the Tan-Lu Fault Zone used in this study can be accessed via DOI: https://doi.org/10.6038/cjg2022Q0336. The focal mechanism data for the Feidong earthquake sequence used in this study can be found in Appendix 1 of this paper. The code for independently selecting fault planes and inverting stress field parameters using the linearization method can be accessed via DOI: https://doi.org/10.6038/cjg2023R0193. The iterative linear stress inversion code (STRESSINVERSE) used for determining stress state and fault planes is available at https://www.ig.cas.cz/stress-inverse/. The code for improved DBSCAN algorithm for automatic fault identification is available at https://github.com/zhangsuxiang/-DBSCAN-. The code for selecting the fault plane that is closest to the given seismogenic fault based on the focal mechanism solution is available at https://github.com/zhangsuxiang/-.

References

Barbot, S. (2019). Slow-slip, slow earthquakes, period-two cycles, full and partial ruptures, and deterministic chaos in a single asperity fault. Tectonophysics, 768(5), 228171.

https://doi.org/10.1016/j.tecto.2019.228171.
Chang, C. D., Lee, J. B., &Kang, T. S. (2010). Interaction between regional stress state and faults: Complementary analysis of borehole in situ stress and earthquake focal mechanism in southeastern Korea. Tectonophysics, 485(1-4), 164-177. https://doi.org/10.1016/j.tecto.2009.12.012.
Chen, H. (2022). Study of crustal deformation characteristics in the central and southern segments of the Tan-Lu Fault Zone based on Anhui CORS. Hefei University of Technology. https://doi:10.27101/d.cnki.ghfgu.2022.001444.
Custódio, S., Lima, V., Vales, D., et al. (2016). Imaging active faulting in a region of distributed deformation from the joint clustering of focal mechanisms and hypocentres: Application to the Azores–western mediterranean region. Tectonophysics, 676, 70-89. https://doi.org/10.1016/j.tecto.2016.03.013.
Ellsworth, W. L. (2013). Injection-induced earthquakes. Science, 341(6142), 1225942. https://doi.org/10.1126/science.1225942.
Fang, H. J., Yao, H. J., Zhang, H. J., et al. (2015). Direct inversion of surface wave dispersion for three-dimensional shallow crustal structure based on ray tracing: methodology and application. Geophysical Journal International, 201(3), 1251-1263. https://doi.org/10.1093/gji/ggv090.
Faulkner, D. R., Mitchell, T. M., Healy, D., et al. (2006). Slip on 'weak' faults by the rotation of regional stress in the fracture damage zone. Nature, 444, 922-925. https://doi.org/10.1038/nature05377.
Fu, X. (2021). The genesis of intermediate and acidic rocks in the southern segment of the Tan-Lu Fault Zone and their implications for regional uplift in the Feidong Area. Hefei University of Technology. https://doi:10.27101/d.cnki.ghfgu.2021.001828.
Guiraud, M., Laborade, O., Philip, H. (1989). Characterizattion of various types of deformation and their corresponding deviatoric stress tensors using microfault analysis. Tectonophysics, 170(3-4), 289-316. https://doi.org/10.1016/0040-1951(89)90277-1.
Guo, H., Zhang, H. J., Froment, B. (2018). Structural control on earthquake behaviors revealed by high-resolution Vp/Vs imaging along the Gofar transform fault, East Pacific Rise. Earth and Planetary Science Letters, 499, 243-255, https://doi.org/10.1016/j.epsl.2018.07.037.
Han, S. C., Zhang, H. J., Xin, H. L., et al. (2022). USTClitho2.0: Updated unified seismic tomography models for continental China lithosphere from joint inversion of body-wave arrival times and surface-wave dispersion data. Seismological Research Letters, 93(1), 201-215. https://doi.org/10.1785/0220210122.
Hardebeck, J. L., Hauksson, E. (2001). Crustal stress field in southern California and its implications for fault mechanics. Journal of Geophysical Research: Solid Earth, 106(B10), 21859-21882. https://doi.org/10.1029/2001JB000292.
Hardebeck, J. L. (2002). A new method for determining first-motion focal mechanisms. Bulletin of the Seismological Society of America, 92(6), 2264-2276. https://doi.org/10.1785/0120010200.
Hardebeck, J. L. (2003). Using S/P amplitude ratios to constrain the focal mechanisms of small earthquakes. Bulletin of the Seismological Society of America, 93(6), 2434-2444. https://doi.org/10.1785/0120020236.
Hu, C. B., Cai, Y. E., Liu, M., et al. (2013). Aftershocks due to property variations in the fault zone:

A mechanical model. Tectonophysics, 588, 179-188. https://doi.org/10.1016/j.tecto.2012.12.013.

Kim, D., Jung, H., Lee, J. (2023). Impact of chlorite dehydration on intermediate-depth earthquakes in subducting slabs. Commun Earth Environ , 4(1), 491. https://doi.org/10.1038/s43247-023-01133-5.

Liu, M., Tan, Y. J., Guo, H., et al. (2025). Fluids and fault structures underlying the complex foreshock sequence of the 2021 MW6.1 Yangbi earthquake. Earth and Planetary Science Letters, 651, 119173. https://doi.org/10.1016/j.epsl.2024.119173.

Wang, H., Cao, J. L., Xu, H. C. (2019). Preliminary application of focal mechanism solutions of small and medium-size earthquakes to fault stability analysis in the southeastern Tibetan plateau. Seismology and Geology, 41(3), 633-648. doi: 10.3969/j.issn.0253-4967.2019.03.007.

Wessel, P., Smith, W. H. F. (1991). Free software helps map and display data. EOS Transactions American Geophysical Union, 72(41), 441-446. https://doi.org/10.1029/90EO00319.

Li, L. L., Huang, X. L., Yao, H. J., et al. (2020). Shallow shear wave velocity structure from ambient noise tomography in Hefei city and its implication for urban sedimentary environment. Chinese Journal of Geophysics (in Chinese), 63(9), 3307-3323. doi: 10.6038/cjg2020O0097.

Liu, B. J., Feng, S. Y., Ji, J.F., et al. (2015). Fine lithosphere structure beneath the middle-southern segment of the Tan-Lu fault zone. Chinese Journal of Geophysics (in Chinese), 58(5), 1610-1621. doi: 10.6038/cjg20150513.

Li, X., Zhao, Y., Liu, B. et al. (2010). Structural deformation and fault activity of the Tan-Lu Fault zone in the Bohai Sea since the late Pleistocene. Chin. Sci. Bull, 55, 1908-1916. https://doi.org/10.1007/s11434-010-3073-z.

Li, Z. Y., Wan, Y. G., Guo, X.Y., et al. (2024). Significance of accurate selection of the seismogenic faults from the earthquake focal mechanisms for stress field reconstruction. Chinese Journal of Geophysics (in Chinese), 67(7), 2612-2624. doi: 10.6038/cjg2023R0193.

Lund, B., Townend, J. (2007). Calculating horizontal stress orientations with full or partial knowledge of the tectonic stress tensor. Geophysical Journal International，170(3), 1328-1335. https://doi.org/10.1111/j.1365-246X.2007.03468.x.

Luo, Y., Zhao, L., Zeng, X. F., et al. (2015). Focal mechanisms of the Lushan earthquake sequence and spatial variation of the stress field. Science China Earth Sciences, 58(7), 1148-1158. https://doi.org/10.1007/s11430-014-5017-y.

Martínez-Díaz, J. J. (2002). Stress field variation related to fault interaction in a reverse oblique-slip fault: the Alhama de Murcia fault, Betic Cordillera, Spain. Tectonophysics, 356(4), 291-305. https://doi.org/10.1016/S0040-1951(02)00400-6.

Michael, A. J. (1984). Determination of stress from slip data: faults and folds. Journal of Geophysical Research: Solid Earth, 89(B13), 11517-11526. https://doi.org/10.1029/JB089iB13p11517.

Morley, C. K., Nixon, C. W. (2016). Topological characteristics of simple and complex normal fault networks. Journal of Structural Geology, 84, 68-84. https://doi.org/10.1016/j.jsg.2016.01.005.

Ni, H. Y., Li, J. L., Yao, H. J., et al. (2025). Preliminary study of the tectonic structure and seismogenic environment of the M4.7 Feidong earthquake sequence on september 18, 2024

in Hefei. Earthquake Science, 38. doi: 10.1016/j.eqs.2024.11.001.
Ozawa, S., Ryosuke A. (2021). Mainshock and aftershock sequence simulation in geometrically complex fault zones. Geophysical Research: Solid Earth, 126(2), e2020JB020865. https://doi.org/10.1029/2020JB020865.
Philibosian, B., Meltzner, A. J. (2020). Segmentation and supercycles: A catalog of earthquake rupture patterns from the Sumatran Sunda Megathrust and other well-studied faults worldwide. Quaternary Science Reviews, 241, 106390. https://doi.org/10.1016/j.quascirev.2020.106390.
Rybicki, K., Kato, T., Kasahara, K. (1985). Mechanism interaction between neighboring active faults static and dynamic stress field induced by faulting. Bulletin of the Earthquake Research Institute University of Tokyo, 60, 1-21. https://doi.org/10.1016/0040-1951(87)90016-3
Get rights and content.
Shao, B., Hou, G. T. (2019). The interactions of fault patterns and stress fields during active faulting in Central North China Block: Insights from numerical simulations. Plos One, 14(4), 1-16. https://doi.org/10.1371/journal.pone.0215893.
Shi, Y. T., Gao, Y. (2022). Spatial distribution of shear wave splitting of the upper crust in the central South China block. Chinese Journal of Geophysics (in Chinese), 65(9), 3268-3279. doi: 10.6038/cjg2022P0741.
Snoke, J. A., Munsey, J. W., Teague, A. C. (1984). A program for focal mechanism determination by combined use of polarity and SV-P amplitude ratio data. Earthquake Notes, 55(3), 15.
Snoke, J. A. (2003). FOCMEC: Focal mechanism determinations. International Geophysics, 81(B), 1629-1630. doi:10.1016/S0074-6142(03)80291-7.
Terakawa, T., Zoporowski, A., Deichmann, N. (2012). High fluid pressure and triggered earthquakes in the enhanced geothermal system in Basel, Switzerland. J Geophys Res, 117, B07305. https://doi.org/10.1029/2011JB008980.
Terakawa, T., Zoporowski, A., Galvan, B., et al. (2010). High-pressure fluid at hypocentral depths in the L'Aquia region inferred from earthquake focal mechanisms. Geology, 38, 995-998. https://doi.org/10.1130/G31457.1.
Vavryčuk, V. (2014). Iterative joint inversion for stress and fault orientations from focal mechanisms. Geophysical Journal International, 199, 69-77. https://doi.org/10.1093/gji/ggu224.
Waldhauser, F., Ellsworth, W. L. (2000). A double-difference earthquake location algorithm: method and application to the northern Hayward fault, California. Bull Seismol Soc Am, 90(6), 1353-1368. https://doi.org/10.1785/0120000006.
Wan, Y. G. (2020). Simulation on relationship between stress regimes and focal mechanisms of earthquakes. Chinese Journal of Geophysics (in Chinese), 63(6), 2281-2296. doi: 10.6038/cjg2020M0472.
Wan, Y. G., Sheng, S. Z., Huang, J. C., et al. (2016). The grid search algorithm of tectonic stress tensor based on focal mechanism data and its application in the boundary zone of China, Vietnam and Laos. Journal of Earth Science, 27(5), 777-785. https://doi.org/10.1007/s12583-015-0649-1.
Xu, X. (2022). Inversion of the tectonic stress field and dynamic interpretation in Anhui region. Institute of Disaster Prevention Science and Technology. doi:10.27899/d.cnki.gfzkj.2022.000025.

Yang, Z. G., Dai, D. Q., Zhang, Y. (2022). Rupture process and aftershock focal mechanisms of the 2022 M6.8 Luding earthquake in Sichuan. Earthquake Science, 35(6), 474-484. https://doi.org/10.1016/j.eqs.2022.12.005.

Yin, G. Y., Zhang, H., Gong, L. W. et al. (2024). Seismic and geological evidence of hidden faults in the Yingpan Reservoir area based on a dense seismic array. Science China Earth Science, 67(7), 2401-2407. https://doi.org/10.1007/s11430-023-1361-4.

Zhang, G. W., Ji, Y., Guo, H., et al. (2022). Complex fault geometry of the 1976 MS7.8 Tangshan earthquake source region in North China. Tectonophysics, 845, 22642. https://doi.org/10.1016/j.tecto.2022.229642.

Zhang, J. D., Yang, C. C., Liu, C. Z., et al. (2010). The deep structures of strike-slip and extension faults and their composite relationship in the southern segment of Tanlu fault zone. Chinese Journal of Geophysics (in Chinese), 53(4), 864-873. doi: 10.3969/j.issn.0001-5733.2010.04.011.

Zhang, S. X. (2024). Stress state of main faults in Tangshan area. Journal of Geodesy and Geodynamics, 44(9), 910-918. doi:10.14075/j.jgg.2023.11.117.

Zhang, S. X., Sheng, S. Z., Xi, B., et al. (2022). Automatic fault identification method based on improved DBSCAN algorithm and its application to Tangshan area. Seismology and Geology, 44(6), 1615-1633. doi: 10.3969/j.issn.0253-4967.2022.06.015.

Zhang, Y. P., Wang, W. T., Yang, W., et al. (2023). Three-dimensional crustal velocity structure beneath the southern segment of the Tan-Lu fault revealed by joint inversion from multi-source data. Chinese Journal of Geophysics (in Chinese), 66(6), 2404-2419. doi: 10.6038/cjg2022Q0336.

Zion, Y. B., Sammis, C. G. (2003). Characterization of Fault Zones. Pure and applied geophysics, 160, 677-715. https://doi.org/10.1007/PL00012554.

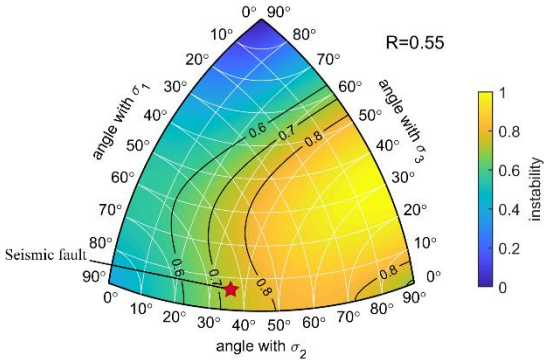

Appendix figure 1. Schematic of the instability of the seismogenic structure of the Feidong earthquake sequence in the principal stress axis coordinate system (Li et al., 2023)

Appendix table 1. Focal mechanism inversion results of earthquakes within the seismogenic structures

data	time	lon/(°E)	lat/(°N)	depth/(km)	M_L	strike/(°)	dip/(°)	rake/(°)	method
2024-2-24	18:13	117.60	31.98	10	4.2	44	81	180	CAP
2024-9-14	05:12	117.60	31.98	10	4.4	230	84	177	CAP
2024-9-18	20:08	117.60	31.97	10	5.2	227	79	170	CAP
2024-9-25	19:29	117.61	31.98	10	4.3	46	89	-177	CAP
2024-10-01	16:34	117.61	31.98	10	4.0	235	65	-171	CAP
2024-9-25	19:58	117.61	31.98	10	3.2	214	50	107	HASH
2024-9-26	15:04	117.61	31.98	10	3.1	192	8	-180	HASH
2024-9-19	15:44	117.61	31.98	10	3.0	90	80	-119	HASH
2024-9-21	16:14	117.61	31.98	10	3.0	210	62	151	HASH
2024-9-25	19:53	117.61	31.98	10	3.0	204	35	110	HASH
2024-9-20	10:46	117.61	31.98	10	2.9	52	23	-101	HASH
2024-10-1	16:28	117.61	31.98	10	2.8	49	42	-39	HASH
2024-9-19	17:25	117.61	31.97	10	2.7	66	69	-98	HASH
2024-4-15	14:26	117.60	31.98	10	2.6	26	79	-23	HASH
2024-9-19	17:56	117.61	31.97	10	2.6	33	81	-137	HASH
2024-9-23	6:40	117.59	31.97	10	2.6	126	72	69	HASH
2024-5-14	2:44	117.60	31.98	10	2.5	41	55	120	HASH
2024-9-18	14:24	117.60	31.97	10	2.5	10	35	165	HASH
2024-9-20	13:46	117.61	31.98	10	2.5	105	35	27	HASH
2024-10-4	12:21	117.61	31.98	10	2.5	16	22	-64	HASH